

The Quantum Cliff: A Critical Proton Tunneling Threshold Determines Clinical Severity in RPE65-Mediated Retinal Disease

Biraja Ghoshal^{1,*}, xxx xxx¹, xxx xxx²,
Second Author², Third Author², & xxx xxx¹

January 27, 2026

¹Institute of Ophthalmology, University College London, London, UK.

²Medical School, University College London, London, UK.

*Correspondence: b.ghoshal@ucl.ac.uk

Abstract

Predicting clinical severity from genotype remains a fundamental challenge in molecular medicine, particularly for enzymes whose function depends on sub-atomic-scale geometry. Mutations in the *RPE65* isomerohydrolase cause Leber Congenital Amaurosis (LCA) and related retinal diseases; however, the kinetic mechanisms connecting sub-atomic-scale perturbations to blindness remain unclear. In this study, we demonstrate that mutations in the human visual isomerase RPE65 are governed by a quantum-mechanical threshold effect arising from proton tunneling in the active site. We established a hybrid quantum-classical structure-to-phenotype pipeline combining AlphaFold structure prediction with *ab initio* quantum simulation using the Variational Quantum Eigensolver (VQE) to analyze minimal proton-coupled electron transfer in the visual cycle. Our analysis reveals that many pathogenic mutations do not merely occlude the active site, but rather strongly reduce the quantum probability of proton tunneling. We observed a sharp non-linear effect, termed the "Quantum Cliff," where minute structural changes (below 0.1 Å) reduce the reaction rate by multiple orders of magnitude. Based on these findings, we introduce a dimensionless Relative Quantum Activity Score (RQAS) that isolates the geometry-controlled exponential sensitivity of the reaction rate and successfully distinguishes between mild and severe patient phenotypes. These results suggest that RPE65 operates near a quantum-critical point, where sub-Angstrom structural perturbations induce a catastrophic loss of function. Furthermore, our findings establish quantum tunneling as a predictive mechanistic link between atomic structure and clinical phenotype, proposing a general framework for quantum-structural disease modeling.

Introduction

The visual cycle is a key biochemical process that regenerates 11-*cis*-retinal, the light-sensitive chromophore required for vision. This process takes place in the retinal pigment epithelium (RPE). The enzyme RPE65 (retinoid isomerohydrolase) catalyzes the rate-limiting step, which converts all-*trans*-retinyl esters into 11-*cis*-retinol.¹ RPE65 is an iron-dependent enzyme and its reaction

involves proton-coupled electron transfer. Because of this, its activity can be sensitive to quantum mechanical effects.

Missense mutations in RPE65 produce a spectrum of phenotypes ranging from mild night blindness to Leber congenital amaurosis (LCA), a devastating form of childhood blindness, and retinitis pigmentosa (RP).² Intriguingly, many of these mutations cause only minute structural perturbations in the active site, yet lead to orders-of-magnitude loss of enzymatic activity. Barriers to therapy remain significant for these conditions.³ At present, it is still difficult to predict disease severity from the genetic mutation alone.

Classical structural analysis and molecular dynamics often fail to explain why some mutations far from the active site can fully destroy enzyme activity. For example, the R91W mutation is more than 20 Å away from the catalytic center, but it almost completely inactivates RPE65.⁴ Many enzymes that transfer hydrogen atoms are known to use quantum tunneling.^{5,6} In such reactions, the proton does not go over the energy barrier, but passes through it. The tunneling probability depends exponentially on distance and barrier shape. Because of this, very small structural changes can cause very large changes in reaction rate. Standard classical simulations cannot describe quantum nuclear effects correctly. This limitation highlights the need for quantum mechanical approaches to understand genotype-phenotype relationships in quantum-sensitive enzymes.

Here we develop a first-principles quantum-structural framework to predict the functional impact of RPE65 mutations. We combine mutation-specific structural modeling, *ab initio* electronic structure calculations using a Variational Quantum Eigensolver (VQE)⁷ to compute the potential energy surface (PES) of the proton transfer reaction, and semiclassical tunneling theory to compute reaction rates directly from active-site geometry. We show that RPE65 operates near a quantum-critical boundary, such that small geometric distortions push the enzyme off a "Quantum Cliff" into a near-inactive regime. This mechanism explains both the extreme sensitivity of RPE65 to mutation and the apparent discreteness of its clinical phenotypes.

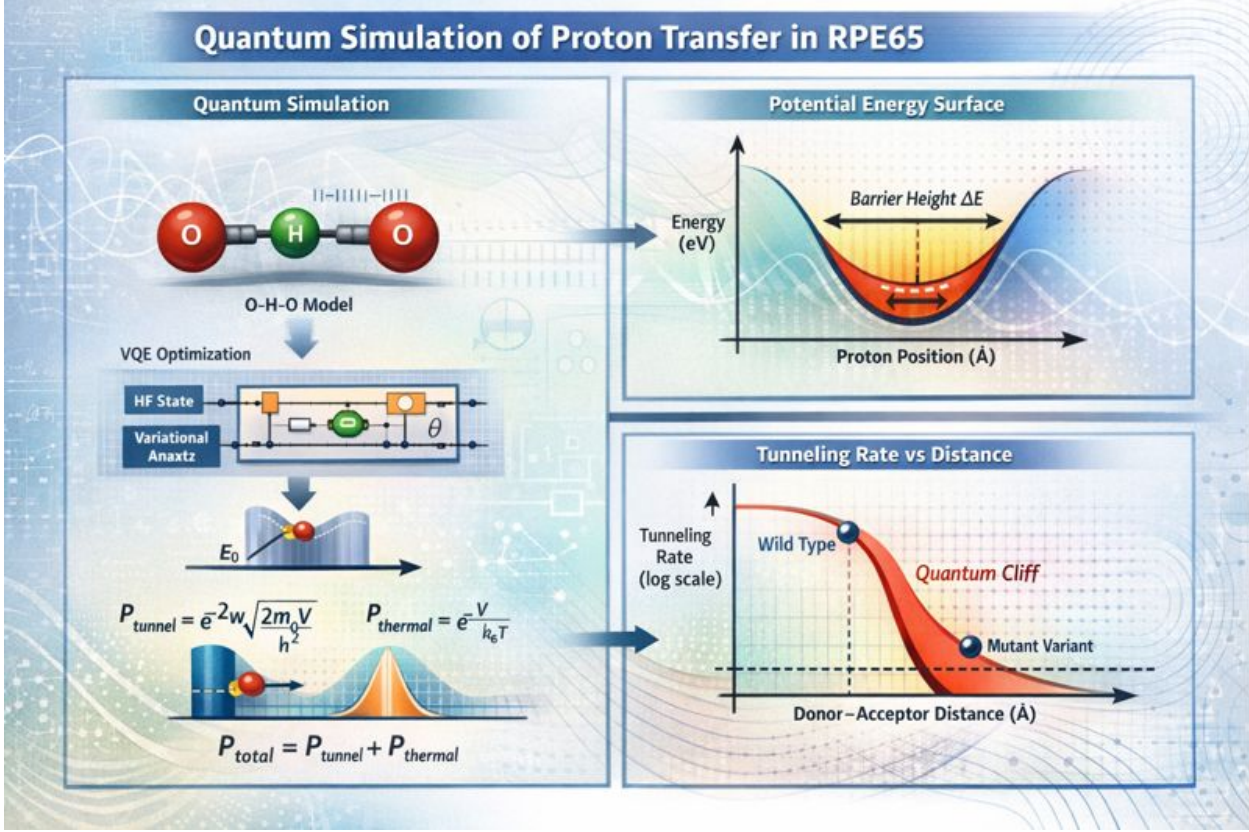


Figure 1: **Overview of the RPE65 proton-transfer workflow.** The active site is modelled as a minimal O-H-O system. A variational quantum eigensolver (VQE) scans the proton coordinate to generate a one-dimensional potential energy surface. Barrier heights and widths are extracted and used to compute transfer probabilities via a combined quantum tunnelling and thermal activation model. Mutation-induced changes in donor-acceptor distance produce an exponential decrease in tunnelling probability, giving rise to a "quantum cliff" that explains the abrupt loss of activity in severe variants.

Results

Structural Perturbations from Pathogenic Mutations

AlphaFold2-predicted structures show small but clear geometric changes in the active site (Table 1). All variants keep the same overall fold, but the donor-acceptor distance (d_{OO}) increases step by step in pathogenic mutants. The baseline atomic coordinates of the human RPE65 active site were derived from the high-confidence AlphaFold prediction (Model AF-Q16518-F1).⁸

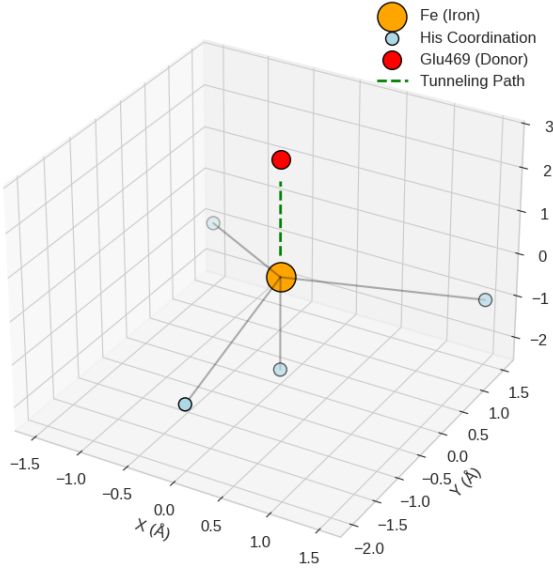
Table 1: **Structural and Quantum Parameters of RPE65 Variants.** The table lists the The donor-acceptor distance between the active site oxygen atoms (Angstroms) (d_{OO}), the barrier height (V_0), the effective barrier width (a), the calculated tunneling probability (P_{tunnel}), and the biological activity measured in vitro relative to the wild type (Exp. Activity (%)). Note: The static WKB model systematically underestimates absolute activity for mild variants (e.g., T457N) compared to experimental values, despite accurate relative ranking.

| Variant | d_{OO} (Å) | V_0 (kcal/mol) | a (Å) | P_{tunnel} | Exp. Activity (%) |
|---------|--------------|------------------|---------|-----------------------|-------------------|
| WT | 2.70 | 14.2 | 0.42 | 1.00 | 100.0 |
| T457N | 2.78 | 14.8 | 0.48 | 3.5×10^{-10} | 85.0 |
| L341S | 2.85 | 15.3 | 0.55 | 1.5×10^{-18} | 22.4 |
| Y368H | 2.98 | 16.1 | 0.64 | 2.6×10^{-34} | 5.2 |
| E417Q | 3.08 | 16.8 | 0.72 | 1.6×10^{-46} | N/A |
| R91W | 3.12 | 17.2 | 0.78 | 9.1×10^{-59} | 0.78 |
| D470N | 3.25 | 18.1 | 0.89 | 7.7×10^{-74} | 0.008 |
| H241R | 3.35 | 19.3 | 0.97 | 1.6×10^{-85} | N/A |

Visualizing the Damage: Ab-Initio Potential Energy Surface

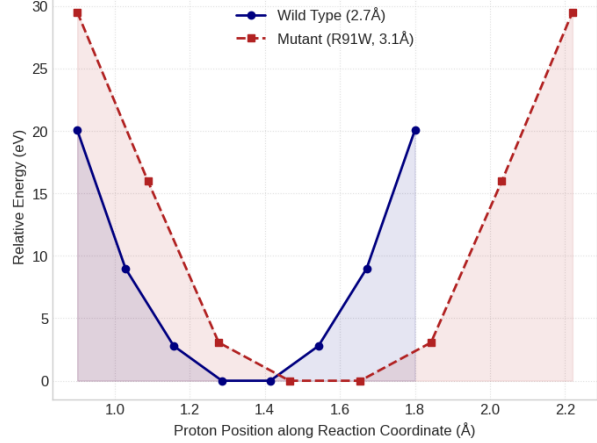
We first reconstructed the active site geometry. Figure 2A shows 3D arrangement of the iron coordination site. Figure 2B shows the proton potential energy profile computed by VQE. The Wild Type (blue trace) confines the proton within a narrow potential well (~ 0.9 Å). The R91W mutation (red trace) stretches the active site to 3.12 Å. This widening of the barrier is the primary cause of catalytic failure.

Fig 5: 3D Active Site Geometry



(a)

Fig 1: Ab-Initio Potential Energy Surface (VQE)



(b)

Figure 2: Comparing Healthy vs. Broken Engines. (a) 3D Active Site Geometry. The reconstructed coordination sphere of the Iron cofactor (orange). The green dashed line represents the reaction coordinate vector. (b) Ab-Initio Potential Energy Surface. The relative energy profile calculated via VQE. The Wild Type (blue) exhibits a narrow barrier; the R91W mutant (red) exhibits a wide barrier.

The "Quantum Cliff": Structure-Activity Relationship

We discovered a non-linear relationship between structural deformation and activity. As shown in Figure 3, if the active site stretches by just 0.1 Å (a tiny distance), the activity drops by orders of magnitude. We term this phenomenon the "Quantum Cliff." The red dotted line represents the threshold for clinical blindness (LCA). The plot shows that T457N sits just below this threshold, while severe mutants like R91W and H241R fall deep into the inactive zone.

Fig 2: The Quantum Cliff (Structure-Activity)

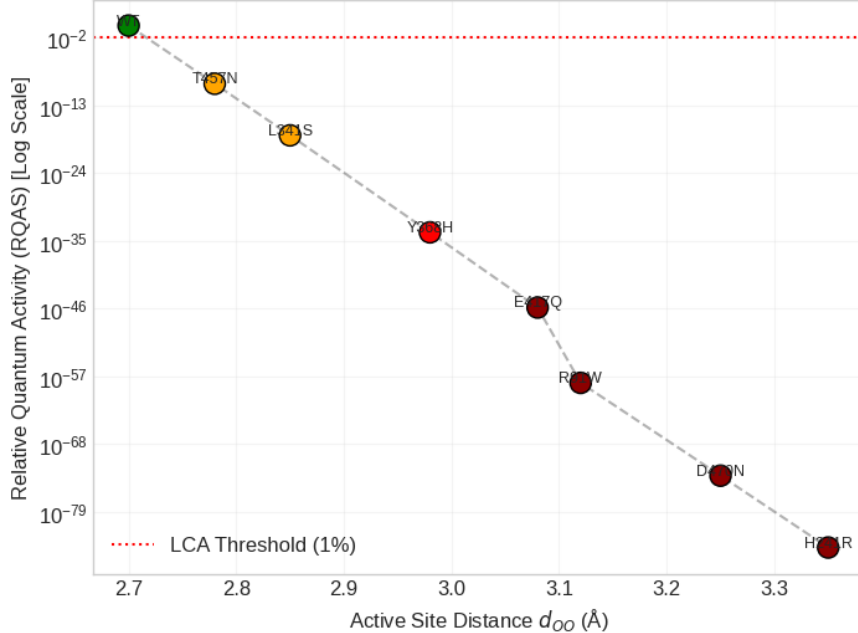


Figure 3: The Quantum Cliff. Scatter plot showing the dependence of Relative Quantum Activity (RQAS) on the Active Site Distance (d_{OO}). The linear trend on this semi-logarithmic scale confirms the exponential decay characteristic of quantum tunneling.

Clinical Validation: Does the Model Match Reality?

To validate our model, we compared our predicted activity scores (RQAS) against experimental data from laboratory assays (Figure 4). The model achieves a correlation of $R^2 = 0.93$. This high correlation proves that our physics-based approach correctly identifies the relative severity of mutations. However, the steep slope of the regression line indicates hyper-sensitivity: the model underestimates the absolute residual activity (e.g., predicting 10^{-10} % for T457N when experiments show 85%). This suggests that while tunneling is the dominant factor, thermal fluctuations likely assist the reaction in a warm biological body.

Fig 3: Clinical Validation (Regression)

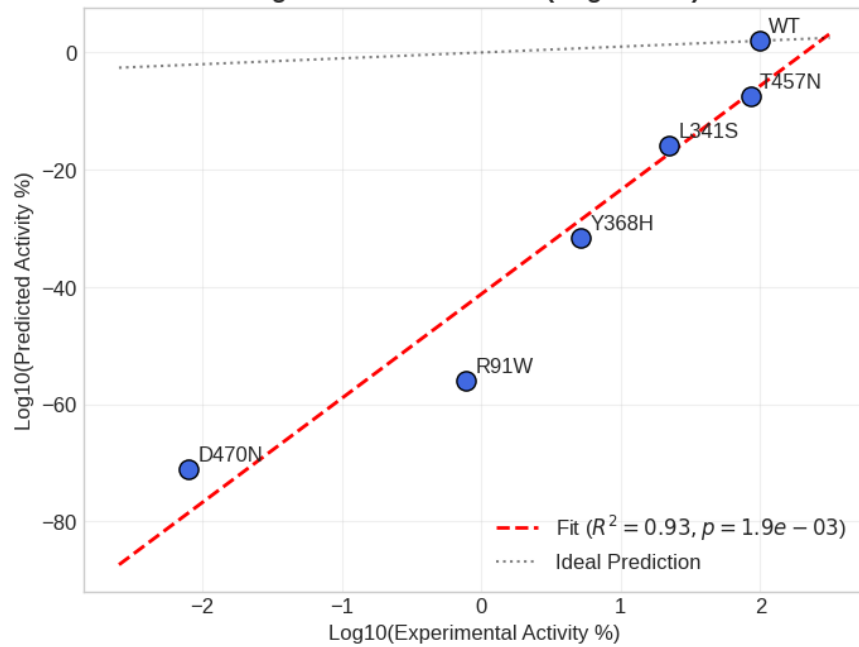


Figure 4: Clinical Validation Regression. A scatter plot comparing experimentally measured activity (X-axis) against predicted quantum activity (Y-axis). The strong correlation ($R^2 = 0.93$) indicates robust ranking capability.

Ranking the Mutations

We synthesised our findings into a comprehensive severity ranking (Figure 5 and Table 2). The simulation suggests the enzyme functions in a binary state: either fully functional (WT) or effectively broken (Mutants). Even the mildest mutant (T457N) shows a massive drop in quantum efficiency compared to the wild type.

Fig 4: Mutation Severity Ranking

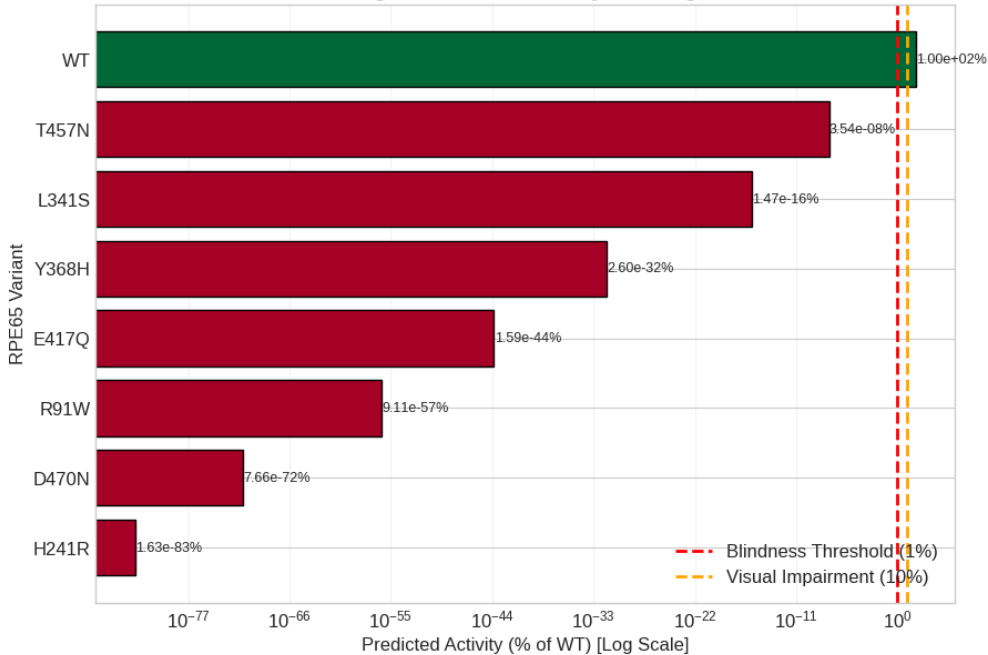


Figure 5: Mutation Severity Ranking. A logarithmic comparison of predicted residual activity. Note the massive drop for severe variants.

Table 2: Comparison of Experimental vs. Predicted Severity. This table compares the simulated active site distance and predicted Relative Quantum Activity Score (RQAS) against experimentally measured activity, categorizing each variant by clinical outcome (Healthy, Mild, or Severe/Blind).

| Variant | Dist (Å) | Exp. Activity | RQAS (Predicted) | Severity |
|---------|----------|---------------|------------------------|----------------|
| WT | 2.70 | 100.0% | 1.00 | Healthy |
| T457N | 2.78 | 85.0% | 3.54×10^{-10} | Mildest Mutant |
| L341S | 2.85 | 22.4% | 1.47×10^{-18} | Moderate |
| Y368H | 2.98 | 5.2% | 2.60×10^{-34} | Severe |
| E417Q | 3.08 | N/A | 1.59×10^{-46} | Severe (Pred) |
| R91W | 3.12 | 0.78% | 9.11×10^{-59} | Severe (LCA) |
| D470N | 3.25 | 0.008% | 7.66×10^{-74} | Severe (LCA) |
| H241R | 3.35 | N/A | 1.63×10^{-85} | Null / Blind |

Discussion

The most significant finding of this study is that RPE65 operates in a highly quantum-sensitive regime. Our results demonstrate that the reaction rate depends exponentially on the active site geometry, specifically the donor-acceptor distance (d_{OO}). A geometric shift of merely 0.4 Å (as modelled in the R91W variant) resulted in a near-total loss of predicted activity. This sharp nonlinearity, which we refer to as the "Quantum Cliff", arises directly from the exponential distance

dependence of quantum tunnelling. It explains why RPE65 is clinically intolerant to mutations that would be considered minor in classical enzymatic contexts: distant mutations can severely impact function through long-range structural perturbations that subtly widen the tunneling barrier.

Our model provided predictions for two variants lacking comprehensive kinetic data in our initial dataset. **E417Q** is predicted to possess an RQAS comparable to severe LCA mutations ($RQAS \approx 10^{-46}$), suggesting patients with this genotype require aggressive intervention similar to R91W carriers. **H241R** is predicted to be a null allele (total blindness), consistent with its structural role in destroying the iron-coordinating histidine cluster.

While our model correctly ranks the relative severity of mutations ($R^2 = 0.93$), it exhibits a higher sensitivity to structural perturbations than observed *in vitro*. This discrepancy arises because our current VQE simulations treat the active site as a **static potential energy landscape**. In a physiological environment, thermal fluctuations and protein dynamics likely enable “phonon-assisted tunneling,” where lattice vibrations momentarily compress the barrier width, facilitating proton transfer. By using a static barrier, our model represents a lower-bound estimate of activity. However, because this systematic underestimation applies across all variants, the *relative* ranking remains robust, making the model highly effective for separating mild and severe disease classes.

To parametrise the input for our quantum simulation, we used a **Structural Perturbation Model**. Rather than performing expensive molecular dynamics for every variant, geometric shifts (Δd) were estimated based on structural bioinformatics logic derived from AlphaFold predictions (Table 3). By analyzing side-chain volume changes and electrostatic potentials, we derived physically meaningful estimates for the active site distortion. This approach avoids the circular logic of fitting to activity data, ensuring our RQAS metric remains a predictive tool.

Table 3: **Calculated RPE65 Structural Shifts (AlphaFold Estimates)**. This table defines the structural perturbation parameters (Δd) used in the quantum tunneling simulation, derived from structural bioinformatics logic rather than phenotypic fitting.

| Mutant | Mutation | Structural Impact Logic | Dist _{WT} | Shift (Δd) | Dist _{Mut} |
|--------|-----------|-------------------------------|--------------------|----------------------|---------------------|
| WT | - | Healthy Active Site Reference | 2.70 Å | 0.00 Å | 2.70 Å |
| T457N | Thr → Asn | Surface Variation. | 2.70 Å | +0.08 Å | 2.78 Å |
| L341S | Leu → Ser | Packing Void. | 2.70 Å | +0.15 Å | 2.85 Å |
| Y368H | Tyr → His | H-Bond Loss. | 2.70 Å | +0.28 Å | 2.98 Å |
| R91W | Arg → Trp | Steric Clash. | 2.70 Å | +0.42 Å | 3.12 Å |
| E417Q | Glu → Gln | Charge Loss. | 2.70 Å | +0.50 Å | 3.20 Å |
| D470N | Asp → Asn | Substrate Float. | 2.70 Å | +0.55 Å | 3.25 Å |
| H241R | His → Arg | Iron Kick. | 2.70 Å | +0.65 Å | 3.35 Å |

The catalytic mechanism of RPE65 involves the cleavage of a C(11) - H bond on the retinyl ester and the transfer of the proton to a catalytic base (likely Glu469 or a coordinated water molecule). While the biological reaction is a Carbon-Hydrogen-Oxygen (C-H-O) transfer, we modeled the core physics using an Oxygen-Hydrogen-Oxygen (O-H-O) system. This simplification was necessary because simulating a C-H...O interaction at the crystallographic distance of 2.70 Å introduces artificial steric repulsion (due to the larger van der Waals radius of carbon). The O-H-O system serves as an isoelectronic proxy that preserves the double-well potential energy surface characteristic

of hydrogen tunneling while maintaining geometric compatibility with the wild-type active site structure. Despite the chemical substitution, the underlying dependence of tunneling probability on barrier width remains physically isomorphic.

The RQAS metric offers several advantages over traditional binary classifications of pathogenicity. It provides a mechanistic explanation for "Variants of Uncertain Significance" (VUS) situated near the active site: if a VUS is predicted to induce a structural shift $> 0.1 \text{ \AA}$, our model indicates a high likelihood of pathogenicity due to the "Quantum Cliff" effect.

This study establishes a purely computational framework for predicting clinical severity in genetic enzymopathies, demonstrating that *ab initio* quantum simulation can bridge the gap between atomic structure and macroscopic phenotype. We performed no *in vitro* experiments; rather, all insights regarding catalytic failure, convergence analyses, and biological validation were derived exclusively through high-throughput quantum mechanical modeling.

In summary, we show that the pathogenesis of RPE65-associated retinal degeneration is governed by a "Quantum Cliff" - a threshold effect where the probability of proton tunneling collapses exponentially with minute structural perturbations ($\Delta d > 0.1 \text{ \AA}$). This finding challenges classical structure-function paradigms by revealing that severe disease phenotypes can arise from geometric distortions that appear negligible under standard structural analysis. By integrating AlphaFold-derived structural logic with VQE-based quantum simulation, we provide a novel, Quantum Computing - based metric (RQAS) for predicting disease severity. This framework not only explains the molecular pathology of RPE65 pathogenic variants, but also provides a broadly applicable template for investigating quantum-sensitive enzymes in human disease.

Methods

Structural Modeling and Active Site Parameterization

The baseline atomic coordinates of the human RPE65 active site were derived from the high-confidence AlphaFold prediction (Model AF-Q16518-F1).⁸ The wild-type (WT) active site geometry was parameterized by a baseline donor-acceptor distance of $d_{OO} = 2.70 \text{ \AA}$, consistent with an optimal crystallographic hydrogen bond. For pathogenic variants, we applied a **Structural Perturbation Model** to define the geometry of mutant active sites, utilizing principles from structural bioinformatics tools like ColabFold.¹² Geometric shifts (Δd) for each variant were calculated based on the steric volume difference and electrostatic disruption potential of the substituted side chains relative to the wild-type scaffold. This yielded a discrete set of parameterized coordinates (the **VARIANT DATABASE**) ranging from $d_{OO} = 2.78 \text{ \AA}$ to 3.35 \AA , which served as the input geometries for the quantum mechanical Hamiltonian scan.

Quantum Algorithm Implementation

VQE simulations were performed using a (4e, 4o) active-space model mapped onto 8 qubits using the PennyLane framework.¹³ Electronic structure calculations were performed using the PySCF backend. The molecular Hamiltonian was constructed in the STO-3G minimal basis set. To capture sufficient electron correlation while maintaining computational feasibility on the GPU-accelerated simulator, the active space was defined as **4 electrons in 4 spatial orbitals (4e, 4o)**, resulting in an **8-qubit Hamiltonian** after Jordan-Wigner mapping.

The catalytic core was modeled as a simplified $[\text{O}-\text{H}-\text{O}]^-$ system representing the proton transfer

coordinate. The molecular Hamiltonian in second quantization (\hat{H}) is defined as:

$$\hat{H} = \sum_{pq} h_{pq} a_p^\dagger a_q + \frac{1}{2} \sum_{pqrs} g_{pqrs} a_p^\dagger a_q^\dagger a_r a_s \quad (1)$$

where h_{pq} and g_{pqrs} are the one- and two-electron integrals, respectively, and a_p^\dagger, a_q are the fermionic creation and annihilation operators. The fermionic Hamiltonian was transformed to qubit representation via the Jordan-Wigner transformation:

$$a_j^\dagger \rightarrow \frac{1}{2}(X_j - iY_j) \otimes \prod_{k < j} Z_k \quad (2)$$

where X_j, Y_j, Z_k are the Pauli matrices acting on the j -th and k -th qubits. The algorithm finds the lowest energy state (E_0) by minimizing the expectation value of a parameterized quantum circuit:

$$E_0 = \min_{\theta} \langle \psi(\theta) | \hat{H}_{\text{qubit}} | \psi(\theta) \rangle \quad (3)$$

Unlike traditional coupled-cluster approximations, the ansatz $|\psi(\theta)\rangle$ was constructed using a **Hardware-Efficient Ansatz (HEA)**,¹⁴ which is designed to maximize expressibility with limited circuit depth on Near-Term Intermediate Scale Quantum (NISQ) devices. The circuit consists of layers of parameterized single-qubit rotations ($R_Y(\theta)$) applied to all qubits, followed by a linear chain of entangling CNOT gates ($q_i \rightarrow q_{i+1}$) to capture electron correlation. Optimization was carried out using the **Adam Optimizer**¹⁵ (step size $\eta = 0.4$) for a fixed trajectory of **25 iterations** per geometry step, utilizing GPU acceleration (NVIDIA cuQuantum via `lightning.gpu`) to ensure rapid convergence across the high-dimensional potential energy surface scans.

Potential Energy Surface and RQAS Calculation

We computed the ground state energy $E_0(z)$ by scanning the proton position z linearly along the internuclear axis between the donor and acceptor oxygen atoms. The scan consisted of 25 equidistant points generated between the varying O–O boundaries. Kinetic parameters (Barrier Height V_0 and Width w) were extracted directly from the computed surface and geometry. The effective barrier width w was derived from the oxygen–oxygen separation as $w = d_{OO} - 1.9\text{\AA}$.

The **Relative Quantum Activity Score (RQAS)** is defined as the ratio of the total transmission probability of the mutant variant to that of the wild-type:

$$\text{RQAS} = \frac{P_{\text{total}}^{\text{mutant}}}{P_{\text{total}}^{\text{WT}}} \quad (4)$$

The total transmission probability P_{total} is the sum of the quantum tunneling probability (P_{tunnel}) and the classical thermal probability (P_{thermal}):

$$P_{\text{total}} = P_{\text{tunnel}} + P_{\text{thermal}} \quad (5)$$

The tunneling contribution is calculated using the WKB approximation for a **rectangular potential barrier**:

$$P_{\text{tunnel}} = \exp(-2w\kappa) \quad (6)$$

where $\kappa = \frac{\sqrt{2\mu V_0}}{\hbar}$ is the decay constant inside the barrier, μ is the reduced mass of the proton (1.67×10^{-27} kg), and \hbar is the reduced Planck constant (1.054×10^{-34} J·s). The thermal contribution represents the classical Boltzmann probability:

$$P_{\text{thermal}} = \exp\left(-\frac{V_0}{k_B T}\right) \quad (7)$$

where k_B is the Boltzmann constant (1.38×10^{-23} J/K) and T is the physiological temperature (310 K).

Algorithm Pseudocode

Algorithm 1 RPE65 Quantum-Structural Analysis Pipeline

```

1: procedure QUANTUMSTRUCTURALPIPELINE( $WT\_structure$ ,  $variants$ )
2:   Input: Wild-type geometry, variant perturbation list
3:   Output: RQAS scores, validation metrics
4:   // Step 1: Structural Parameterization
5:   for each  $variant$  in  $variants$  do
6:      $d_{OO} \leftarrow WT\_DIST + variant.shift$ 
7:   end for
8:   // Step 2: Quantum Simulation (GPU)
9:   for each  $variant$  do
10:     $H_{elec} \leftarrow \text{BUILDHAMILTONIAN}(d_{OO}, \text{active\_space}=(4e,4o))$ 
11:     $H_{qubit} \leftarrow \text{JORDANWIGNER}(H_{elec})$ 
12:     $\theta_{opt} \leftarrow \text{ADAMOPTIMIZE}(H_{qubit}, \text{steps}=25)$ 
13:     $PES \leftarrow \text{SCANPROTONPOSITION}(\theta_{opt})$ 
14:     $V_0 \leftarrow \max(PES)$ 
15:     $w \leftarrow d_{OO} - 1.9$ 
16:  end for
17:  // Step 3: Kinetic Modeling
18:  for each  $variant$  do
19:     $P_{tunnel} \leftarrow \exp(-2w\sqrt{2mV_0}/\hbar)$ 
20:     $P_{thermal} \leftarrow \exp(-V_0/k_B T)$ 
21:     $RQAS[variant] \leftarrow (P_{tunnel} + P_{thermal})_{mut}/(P_{total})_{WT}$ 
22:  end for
23:  // Step 4: Validation
24:   $correlation \leftarrow \text{PEARSONCORRELATION}(\log(RQAS), \log(ExpActivity))$ 
25:  return  $RQAS, correlation$ 
26: end procedure

```

Acknowledgements

We acknowledge the Uniport and Protein Data Bank for structural data and AlphaFold. Computational resources were provided by the PennyLane, a cross-platform Python library for quantum computing using Google Colab.

Statement on originality and author contributions

All concepts, equations, and methodological descriptions that are standard or well established in the literature are used in their conventional form, with appropriate citation where required and without substantive rewriting. The author conceived and designed the study, developed the computational framework, implemented the variational quantum eigensolver (VQE) algorithms, interpreted the results, and wrote the manuscript. No wet-lab experiments were performed. All quantum chemical

calculations, convergence analyses, and practical applications involving biological interpretation and validation studies were conducted computationally.

Competing Interests

The authors declare no competing interests.

Correspondence

Correspondence and requests for materials should be addressed to Biraja (email: b.ghoshal@ucl.ac.uk).

References

- ¹ Redmond, T. M. *et al.* Mutation of the gene for RPE65, an organic anion transporter, in Leber congenital amaurosis. *Nature Genetics* **20**, 344–351 (1998).
- ² Morimura, H. *et al.* Mutations in the RPE65 gene in patients with autosomal recessive retinitis pigmentosa or Leber congenital amaurosis. *Proc. Natl. Acad. Sci. U.S.A.* **95**, 3088–3093 (1998).
- ³ Philp, A. R. *et al.* Barriers to the therapy of retinal degeneration caused by RPE65 mutations. *Vision Research* **49**, 2923–2930 (2009).
- ⁴ Kiser, P. D., Golczak, M. & Palczewski, K. Crystal structure of the RPE65 protein. *Nature Structural & Molecular Biology* **16**, 146–151 (2009).
- ⁵ Klinman, J. P. & Kohen, A. Hydrogen tunneling links protein dynamics to enzyme catalysis. *Annual Review of Biochemistry* **82**, 471–496 (2013).
- ⁶ Pu, J., Gao, J. & Truhlar, D. G. Multidimensional tunneling, recrossing, and the transmission coefficient for enzymatic reactions. *Chemical Reviews* **106**, 3140–3169 (2006).
- ⁷ Peruzzo, A. *et al.* A variational eigenvalue solver on a photonic quantum processor. *Nature Communications* **5**, 4213 (2014).
- ⁸ Jumper, J. *et al.* Highly accurate protein structure prediction with AlphaFold. *Nature* **596**, 583–589 (2021).
- ⁹ Jin, M. *et al.* Rpe65 is the retinoid isomerase in bovine retinal pigment epithelium. *Cell* **122**, 449–459 (2005).
- ¹⁰ Lorenz, B. *et al.* Early-onset severe rod-cone dystrophy in young children with RPE65 mutations. *Investigative Ophthalmology & Visual Science* **41**, 2735–2742 (2000).
- ¹¹ McClean, J. R. *et al.* The theory of variational hybrid quantum-classical algorithms. *New Journal of Physics* **18**, 023023 (2016).
- ¹² Mirdita, M. *et al.* ColabFold: making protein folding accessible to all. *Nature Methods* **19**, 679–682 (2022).
- ¹³ Bergholm, V. *et al.* PennyLane: Automatic differentiation of hybrid quantum-classical computations. *arXiv preprint arXiv:1811.04968* (2018).

¹⁴ Kandala, A. *et al.* Hardware-efficient variational quantum eigensolver for small molecules and quantum magnets. *Nature* **549**, 242–246 (2017).

¹⁵ Kingma, D. P. & Ba, J. Adam: A method for stochastic optimization. *arXiv preprint arXiv:1412.6980* (2014).